

The Relativistic Dirac-Brueckner Approach to Nuclear Matter

Christian Fuchs¹

Institut für Theoretische Physik, Universität Tübingen, D-72076 Tübingen,
Germany

An overview on the relativistic Dirac-Brueckner approach to the nuclear many-body problem is given. Different approximation schemes are discussed, with particular emphasis on the nuclear self-energy and the saturation mechanism of nuclear matter. I will further discuss extensions of the standard approach, amongst other things the inclusion of non-nucleonic degrees of freedom, many-body forces and finally compare relativistic and non-relativistic approaches.

1 Introduction

An *ab initio* description of dense nuclear matter which is based on QCD as the fundamental theory of strong interactions is presently not possible and will not be in the foreseeable future. The reason lies in the highly non-perturbative character of the formation of hadronic bound states and their interactions. Hence a quantitative description of nuclear many-particle systems has to be based on effective theories. Particularly successful are theories which's effective degrees of freedom are hadrons, i.e. nucleons (and their excited states) and mesons. The nucleon-nucleon interaction is thereby described by the exchange of mesons as depicted in Fig. 1. Modern One-Boson-Exchange Potentials (OBEP), as e.g. the Bonn potentials [1, 2], are usually based on the exchange of the six non-strange mesons: σ (scalar, iso-scalar), ω (vector, iso-scalar), ρ (vector, iso-vector), π (pseudo-scalar, iso-vector), η (pseudoscalar, iso-scalar), δ (scalar, iso-vector).

The connection of the hadronic to the QCD world is reflected in the *quark-hadron-duality*. Due to the almost vanishing masses of the light (current) quarks chiral symmetry of the QCD Lagrangian is almost fulfilled. It is, however, spontaneously broken by the large non-vanishing vacuum expectation values of the quark and gluon condensates which are responsible for the finite hadron masses. These condensates which are the basic quantities in the non-perturbative regime of QCD change dramatically in the medium. The connection to the energy density ϵ in terms of hadronic degrees of freedom is in principle given via the Hellmann-Feynman theorem

$$\langle \bar{q}q \rangle_\rho = \langle \bar{q}q \rangle_{\text{vac}} + \frac{1}{2} \sum_h \frac{\partial \epsilon}{\partial h} \frac{\partial m_h}{\partial m_q} \quad (1)$$

where the sum runs over all hadronic contributions h to the energy density ϵ . However, neither this part can uniquely be fixed nor the second part of eq. (1), i.e. the derivatives of the hadron masses with respect to the current quark masses. Thus QCD can help to constrain hadronic theories but an exact mapping of the two worlds is still a dream for the future.

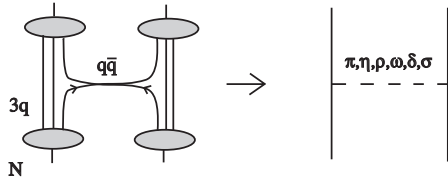


Fig. 1. Schematic representation of the One-Boson-Exchange model for the nucleon-nucleon interaction. The figure is taken from [3].

However, also within hadronic theories a perturbative approach to the strongly interacting nuclear systems is not possible. A systematic summation of diagrams up to infinite order in terms of the Brueckner hole-line expansion turned out to be an appropriate treatment. Already in lowest order which corresponds to standard Brueckner theory the saturation of nuclear matter can be described at least qualitatively [4, 5, 6]. In Brueckner theory the T-matrix (or Brueckner G-matrix) serves as an effective in-medium two-body interaction. It is determined by a self-consistent summation of the ladder diagrams in a quasi-potential approximation (Thompson equation) to the Bethe-Salpeter equation. The character of the bare nucleon-nucleon interaction, in particular the repulsive short range part (hard-core) requires to account for two-body correlations in a self-consistent way. The effect of the correlations on the two-nucleon wave function in the medium is schematically depicted in Fig. 2.

However, non-relativistic Brueckner calculations are not able to meet the empirical saturation point of nuclear matter ($\rho_{\text{sat}} = 0.16 \text{ fm}^{-3}$, $E_{\text{bind}} = -16 \text{ MeV}$). In contrast, the saturation points obtained for various types of NN-potentials were all located on the so-called Coester line [5] (for a recent review see [3]) in the $\epsilon - \rho$ plane. A breakthrough was achieved when first relativistic (Dirac-) Brueckner-Hartree-Fock (DBHF) calculations were performed in the late eighties [7, 8]. Now the Coester line was shifted much closer towards the empirical area of saturation. One reason for the success of the relativistic approach is usually attributed to the fact that the dressing of the in-medium spinors introduces a density dependence to the interaction which is missing in the non-relativistic treatment. In the latter case the inclusion of three-body forces can lead to similar effects. The occurrence of many-body forces is, however, closely connected to the inclusion of non-nucleon degrees of free-

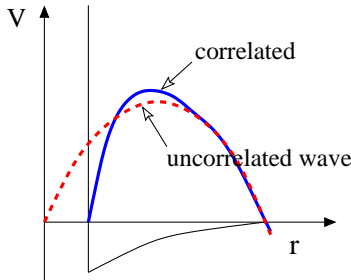


Fig. 2. Effect of the two-body correlations on the two-nucleon wave function as a function of the relative distance r . The nucleon-nucleon potential is schematically indicated. It shows the typical short-range repulsion (hard core) together with the intermediate and long-range attractive parts. The figure is taken from [3].

dom, i.e. resonances. A discussion of these aspects as well as a comparison of relativistic versus non-relativistic approaches will be given in Sec. 5.

Relativistic Brueckner calculations are not straightforward and the approaches of various groups [7, 8, 9, 10, 11, 12, 13, 14] are similar but differ in detail, depending on solution techniques and the particular approximations made. The intention of the present work is to review the *standard* relativistic Brueckner approach and to discuss implications of the several approximation schemes, as well as the role of higher order correlations, Pauli effects, and the special role of Dirac phenomenology.

Large part of the present discussion will be devoted to the determination of the nuclear self-energy. To determine its Lorentz structure and momentum dependence, the T-matrix has to be decomposed into Lorentz components, i.e. scalar, vector, tensor, etc. contributions. This procedure is not free from ambiguities [15]. Due to identical matrix elements for positive energy states pseudo-scalar and pseudo-vector components cannot uniquely be disentangled for on-shell scattering. However, with a pseudo-scalar vertex the pion couples maximally to negative energy states which are not included in the standard Brueckner approach. This is inconsistent with the potentials used since OBEPs are usually based on the no-sea approximation. Hence, pseudo-scalar contributions due to the one- π exchange (OPE) lead to large and spurious contributions from negative energy states. In [11] it was shown that such spurious contributions dominate the momentum dependence of the nuclear self-energy, and, in particular, lead to an artificially strong momentum dependence inside the Fermi sea. It was further demonstrated [11] that previous methods [7, 10] used to cure this problem fail and finally a new and reliable method was proposed to remove those spurious contributions from the T-matrix [12]. If calculations are performed in full Dirac space, i.e. including anti-particles, the complete information on the Lorentz structure of

the self-energy is available but in this case one has to cope with other problems [9, 13, 16, 14].

2 The Relativistic Brueckner Approach

2.1 The Coupled Set of Equations

In the relativistic Brueckner approach the nucleon inside the nuclear medium is viewed as a dressed particle in consequence of its two-body interaction with the surrounding nucleons. The in-medium interaction of the nucleons is treated in the ladder approximation of the relativistic Bethe-Salpeter (BS) equation

$$T = V + i \int V Q G G T \quad , \quad (2)$$

where T denotes the T-matrix. V is the bare nucleon-nucleon interaction. The intermediate off-shell nucleons in the scattering equation are described by a two-particle propagator iGG . The Pauli operator Q accounts for the influence of the medium by the Pauli-principle and projects the intermediate scattering states out of the Fermi sea. The Green's function G fulfills the Dyson equation

$$G = G_0 + G_0 \Sigma G \quad . \quad (3)$$

G_0 denotes the free nucleon propagator while the influence of the surrounding nucleons is expressed by the nucleon self-energy Σ . In Brueckner theory this self-energy is determined by summing up the interaction with all the nucleons inside the Fermi sea in Hartree-Fock approximation

$$\Sigma = -i \int_F (Tr[GT] - GT) \quad . \quad (4)$$

The coupled set of equations (2)-(4) represents a self-consistency problem and has to be iterated until convergence is reached.

Due to translational and rotational invariance, parity conservation and time reversal invariance the self-energy in isospin saturated nuclear matter has the general form $\Sigma = \Sigma_s - \gamma_\mu \Sigma^\mu$. It depends on the Lorentz invariants k^2 , $k \cdot j$ and j^2 , with j_μ and k_μ being the baryon current and the nucleon four-momentum, respectively [17]. The invariants can also be expressed in terms of k_0 , $|\mathbf{k}|$ and k_F , where k_F denotes the Fermi momentum. Furthermore the vector part of the self energy has contributions proportional to k^μ and to the current j^μ . Defining the streaming velocity as $u^\mu = j^\mu / \sqrt{j^2}$, the momentum k^μ can be decomposed into contributions parallel and perpendicular to the streaming velocity, i.e. $k^\mu = (k \cdot u)u^\mu + \Delta^{\mu\nu} k_\nu$ with the projector $\Delta^{\mu\nu} = g^{\mu\nu} - u^\mu u^\nu$. The vector part of the self-energy can then be written covariantly as [10, 13]

$$\Sigma^\mu = \Sigma_o u^\mu + \Sigma_v \Delta^{\mu\nu} k_\nu \quad . \quad (5)$$

Thus the full self-energy reads

$$\Sigma(k, k_F) = \Sigma_s(k, k_F) - \gamma_\mu [\Sigma_o(k, k_F) u^\mu + \Sigma_v(k, k_F) \Delta^{\mu\nu} k_\nu] \quad (6)$$

$$= \Sigma_s(k, k_F) - \gamma_0 \Sigma_o(k, k_F) + \gamma \cdot \mathbf{k} \Sigma_v(k, k_F) |_{\text{RF}} \quad (7)$$

where the subscript RF indicates the respective expressions in the nuclear matter rest frame ($u^\mu = \delta^{\mu 0}$) [7, 18]. The Σ_s , Σ_o and Σ_v components are Lorentz scalar functions which actually depend on $k_0, |\mathbf{k}|$ and k_F . They follow from the self-energy matrix by taking the respective traces [10]

$$\Sigma_s = \frac{1}{4} \text{tr} [\Sigma] \quad (8)$$

$$\Sigma_o = \frac{-1}{4} \text{tr} [\gamma_\mu u^\mu \Sigma] = \frac{-1}{4} \text{tr} [\gamma_0 \Sigma] |_{\text{RF}} \quad (9)$$

$$\Sigma_v = \frac{-1}{4 \Delta^{\mu\nu} k_\mu k_\nu} \text{tr} [\Delta^{\mu\nu} \gamma_\mu k_\nu \Sigma] = \frac{-1}{4 |\mathbf{k}|^2} \text{tr} [\gamma \cdot \mathbf{k} \Sigma] |_{\text{RF}} \quad . \quad (10)$$

The Dirac equation for the in-medium spinor basis can be deduced from the Green's function. Written in terms of effective masses and momenta

$$m^* = M + \text{Re} \Sigma_s \quad , \quad k_\mu^* = k_\mu + \text{Re} \Sigma_\mu \quad (11)$$

the Dirac equation has the form

$$[k^* - m^* - i \text{Im} \Sigma] u(k) = 0. \quad (12)$$

In the following we will work in the quasi-particle approximation and neglect the imaginary part of the self-energy from now on. Thus the effective nucleon four-momentum will be on mass shell even above the Fermi surface, fulfilling the relation $k_\mu^* k^{*\mu} = m^{*2}$. Since we only deal with the real part of the self-energy in the quasi-particle approximation we omit this in the notation. In the nuclear matter rest frame the four-momentum follows from Eq. (11)

$$\mathbf{k}^* = \mathbf{k}(1 + \Sigma_v) \quad , \quad k_0^* = E^* = \sqrt{\mathbf{k}^2(1 + \Sigma_v)^2 + m^{*2}} \quad (13)$$

which allows one to eliminate the Σ_v -term in the Dirac equation,

$$[(\alpha \cdot \mathbf{k}) - \gamma^0 \tilde{m}^*] u(k) = \tilde{E}^* u(k) \quad , \quad (14)$$

by a rescaling of the effective mass and the kinetic energy

$$\tilde{m}^* = \frac{m^*}{1 + \Sigma_v} \quad , \quad \tilde{E}^* = \frac{E^*}{1 + \Sigma_v} = \sqrt{\mathbf{k}^2 + \tilde{m}^{*2}} \quad . \quad (15)$$

The solution of the Dirac equation provide the in-medium nucleon spinor basis

$$u_\lambda(k, k_F) = \sqrt{\frac{\tilde{E}^*(\mathbf{k}) + \tilde{m}_F^*}{2\tilde{m}_F^*}} \begin{pmatrix} 1 \\ \frac{2\lambda|\mathbf{k}|}{\tilde{E}^*(\mathbf{k}) + \tilde{m}_F^*} \end{pmatrix} \chi_\lambda \quad , \quad (16)$$

where $\tilde{E}^*(\mathbf{k}) = \sqrt{\mathbf{k}^2 + \tilde{m}_F^{*2}}$. χ_λ denotes a two-component Pauli spinor with $\lambda = \pm\frac{1}{2}$. The normalization of the Dirac spinor is $\bar{u}_\lambda(k, k_F)u_\lambda(k, k_F) = 1$. Since the in-medium spinor contains the reduced effective mass the matrix elements of the bare nucleon-nucleon interaction become density dependent. From the Dirac equation (14) one derives the relativistic Hamiltonian, i.e. the single-particle potential $\hat{U} = \gamma^0 \Sigma$. The expectation value of \hat{U} , i.e. sandwiching \hat{U} between the effective spinor basis (16), yields the single particle potential

$$U(k) = \frac{\langle u(k) | \gamma^0 \Sigma | u(k) \rangle}{\langle u(k) | u(k) \rangle} = \frac{m^*}{E^*(\mathbf{k})} \langle \bar{u}(k) | \Sigma | u(k) \rangle \quad (17)$$

which can be evaluated as

$$U(k, k_F) = \frac{m^*}{E^*} \Sigma_s - \frac{k_\mu^* \Sigma^\mu}{E^*} \quad (18)$$

$$= \frac{m^* \Sigma_s}{\sqrt{\mathbf{k}^2(1 + \Sigma_v)^2 + m^{*2}}} - \Sigma_o + \frac{(1 + \Sigma_v) \Sigma_v \mathbf{k}^2}{\sqrt{\mathbf{k}^2(1 + \Sigma_v)^2 + m^{*2}}} \quad . \quad (19)$$

In many applications [8, 19] the single particle potential is only given in terms of a scalar and zero-vector component. This can be achieved by introducing reduced fields $\tilde{\Sigma}_s$ and $\tilde{\Sigma}_o$ as

$$\tilde{\Sigma}_s = \tilde{m}^* - M = \frac{\Sigma_s - \Sigma_v M}{1 + \Sigma_v} \quad , \quad \tilde{\Sigma}_o = \tilde{E}^* - E = \Sigma_o - \tilde{E}^*(\mathbf{k}) \Sigma_v \quad . \quad (20)$$

The single particle potential has then the form

$$U(k, k_F) = \frac{\tilde{m}^*}{E^*} \tilde{\Sigma}_s - \tilde{\Sigma}_o \quad . \quad (21)$$

Frequently the reduced fields, Eq. (20), are used rather than the projected components since they represent the self-energy in a mean field or Hartree form. Thus they can easily be related to effective hadron mean field theory [20, 21]. Such a representation is meaningful since the Σ_v -contribution is a moderate correction.

2.2 The In-Medium T-Matrix

Before going into details I will shortly summarize the main assumptions which are made in the *standard* relativistic Brueckner approach to solve the BS-equation (2):

- *No sea approximation.* The subspace of negative energy states is omitted. In this way one avoids the delicate problem of infinities which would generally appear due to contributions from negative energy nucleons in the Dirac sea. The approximation is consistent with the usage of standard OBE potentials which are derived under the same assumption.
- *Thompson choice.* The full two-body propagator iGG in the BS-equation is replaced by an effective two-body propagator propagator. The Thompson propagator (and similar the Blankenbecler sugar propagator) projects the intermediate nucleons onto positive energy states and restricts the exchanged energy transfer by $\delta(k^0)$ to zero. Thus the BS-equation is reduced to a three dimensional integral equation of the Lippmann-Schwinger type, the so called Thompson equation [22].
- *Reference spectrums approximation.* The momentum dependent effective mass \tilde{m}^* which enters into the Thompson propagator is replaced by an average value \tilde{m}_F^* (averaged over the Fermi sea). The approximation is justified as long as the self-energy exhibits a weak momentum dependence.
- *Angle-averaged Pauli operator.* The Pauli operator is replaced by its angle-averaged counterpart which allows to solve the Thompson equation in a decoupled angular-momentum partial wave basis.
- *Quasi-particle approximation.* The T-matrix is determined for on-shell scattering at the quasi-particle pole. Finite width spectral functions are not taken into account.

In contrast to the self-energy, Eq. (4), which has to be calculated in the nuclear matter rest frame, the Thompson Eq. (23) is most naturally solved in the two-nucleon c.m. frame. The Thompson propagator and similar the Blankenbecler-Sugar propagator imply that the time-like component of the momentum transfer in V and T is set equal to zero which is a natural constraint in the c.m. frame, however, not a covariant one. The Thompson equation reads in the c.m. frame

$$T(\mathbf{p}, \mathbf{q}, x)|_{c.m.} = V(\mathbf{p}, \mathbf{q}) \quad (22)$$

$$+ \int \frac{d^3\mathbf{k}}{(2\pi)^3} V(\mathbf{p}, \mathbf{k}) \frac{\tilde{m}_F^{*2}}{\tilde{E}^{*2}(\mathbf{k})} \frac{Q(\mathbf{k}, x)}{2\tilde{E}^*(\mathbf{q}) - 2\tilde{E}^*(\mathbf{k}) + i\epsilon} T(\mathbf{k}, \mathbf{q}, x) \quad ,$$

where $\mathbf{q} = (\mathbf{q}_1 - \mathbf{q}_2)/2$ is the relative three-momentum of the initial state while \mathbf{k} and \mathbf{p} are the relative three-momenta of the intermediate and final states, respectively. The starting energy in Eq. (23) is already fixed by $\sqrt{s^*} = 2\tilde{E}^*(\mathbf{q}) = 2\sqrt{\mathbf{q}^2 + \tilde{m}_F^{*2}}$. If \mathbf{q}_1 and \mathbf{q}_2 are nuclear matter rest frame momenta of the nucleons in the initial state, the boost-velocity \mathbf{u} into the c.m. frame is given by

$$\mathbf{u} = \mathbf{P} / \sqrt{\tilde{s}^* + \mathbf{P}^2} \quad , \quad (23)$$

with the total three-momentum and the invariant mass $\mathbf{P} = \mathbf{q}_1 + \mathbf{q}_2$ and $\tilde{s}^* = (\tilde{E}^*(\mathbf{q}_1) + \tilde{E}^*(\mathbf{q}_2))^2 - \mathbf{P}^2$, respectively. In Eq. (23) x denotes the set of additional parameters $x = \{k_F, \tilde{m}_F^*, |\mathbf{u}|\}$ on which the T-matrix depends.

The Pauli operator Q explicitly depends on the chosen frame, i.e., on the boost 3-velocity \mathbf{u} into the c.m.-frame. The Thompson equation (23) for the on-shell T-matrix ($|\mathbf{p}| = |\mathbf{q}|$) can be solved applying standard techniques described in detail by Erkelenz [23]. Doing so, one constructs the positive-energy helicity T-matrix elements from the $|JMLS\rangle$ -scheme. On-shell only five of the sixteen helicity matrix elements are independent which follows from general symmetries [23]. After a partial wave projection onto the $|JMLS\rangle$ -states the integral reduces to a one-dimensional integral over the relative momentum $|\mathbf{k}|$ and Eq. (23) decouples into three subsystems of integral equations for the uncoupled spin singlet, the uncoupled spin triplet and the coupled triplet states. For this purpose the Pauli operator Q has to be replaced by an angle averaged Pauli operator \bar{Q} [18]. We are solving the integral equations by the matrix inversion techniques of Haftel and Tabakin [24]. Real and imaginary parts of the T-matrix are calculated separately by the principal-value treatment given in Ref. [25]. Due to the anti-symmetry of the two-fermion states the total isospin I of the two-nucleon system ($I=0,1$) can be restored by the selection rule:

$$(-)^{L+S+I} = -1 \quad . \quad (24)$$

From the five independent on-shell amplitudes in the $|JMLS\rangle$ -representation the five independent partial wave amplitudes in the helicity representation (for $I=0,1$ and real and imaginary part separately) are obtained by inversion of Eq. (3.32) and then of Eq. (3.28) of Ref. [23]. The summation over the total angular momentum J yields the full helicity matrix element

$$\sum_J \left[\frac{2J+1}{4\pi} \right] d_{\lambda\lambda'}^J(\theta) \langle |\mathbf{p}| \lambda'_1 \lambda'_2 | T^{J,I}(x) | |\mathbf{q}| \lambda_1 \lambda_2 \rangle = \langle \mathbf{p} \lambda'_1 \lambda'_2 \Pi_3 | T(x) | \mathbf{q} \lambda_1 \lambda_2 \Pi_3 \rangle. \quad (25)$$

Here θ is the scattering angle between \mathbf{q} and \mathbf{p} and $\lambda = \lambda_1 - \lambda_2$, $\lambda' = \lambda'_1 - \lambda'_2$. The reduced rotation matrices $d_{\lambda\lambda'}^J(\theta)$ are those defined by Rose [26]. The matrix element (25) is actually independent of the third component of the isospin I_3 .

3 The Nuclear Self-Energy

The easiest way to determine scalar and vector self-energy components directly from the single particle potential U (17). Since U is obtained after complete summation over Dirac-indices of the T-matrix one by this way can avoid cumbersome projection techniques which are required using the trace formulas (8)-(10). Using Eq. (21) a fit to U delivers the density dependent

but *momentum independent* self-energy components $\tilde{\Sigma}_s$ and $\tilde{\Sigma}_o$. This method has e.g. been applied in [8]. An attempt to extend this method and to extract by fitting procedures momentum dependent fields [19] suffered by large uncertainties since one tries then to extract two functions out of one.

A more accurate determination of the density and momentum dependence of the self-energy requires projection techniques for the in-medium T-matrix as outlined first by Horowitz and Serot [18]. That this procedure is also not free from ambiguities has been noticed relatively early [7, 15]. The whole problem arises from the *no sea approximation* in the standard approach. When calculations are performed in full Dirac space [9, 13, 14, 16] the Lorentz structure of the self-energy can uniquely determined from the information available from those matrix elements ($\langle \bar{v} | \Sigma | u \rangle, \langle \bar{v} | \Sigma | v \rangle$) which involve negative energy states. The inclusion of negative energy excitations with 4 states for each spinor yields in total $4^4 = 256$ two-body matrix elements for the T-matrix. Symmetry arguments reduce this to 44 for on-shell particles [27]. If one takes now only positive energy solutions into account this reduces to $2^4 = 16$ two-body matrix elements.

For on-shell matrix elements the number of independent matrix elements can be further reduced by symmetry arguments down to 5. Thus, all on-shell two-body matrix elements can be expanded into five Lorentz invariants. But these five invariants are not uniquely determined since the Dirac matrices involve also negative energy states. The decomposition of a one-body operator into a Lorentz scalar and a Lorentz vector contributions depends therefore on the choice of these five Lorentz invariants.

In nuclear matter the largest ambiguity arises concerning the determination of pseudo-scalar (*ps*) and pseudo-vector (*pv*) T-matrix elements. The *pv* invariant in the medium is defined as

$$PV = \frac{k_2^* - k_1^*}{2m^*} \gamma_5 \otimes \frac{q_2^* - q_1^*}{2m^*} \gamma_5 \quad (26)$$

with k_1^*, q_1^* the initial and k_2^*, q_2^* the final momenta of the scattering particles. For on-shell scattering of positive energy states the *ps* and *pv* matrix elements are identical (using the Dirac eq.)

$$\bar{u}(q) \left(\frac{q^* - p^*}{2m^*} \right) \gamma_5 u(p) = \bar{u}(q) \gamma_5 u(p) \quad . \quad (27)$$

The *ps* vertex couples on the other hand maximally to negative energy whereas the *pv* vertex suppresses the coupling to antiparticles for on-shell scattering

$$\bar{v}(q) \left(\frac{q^* - p^*}{2m^*} \right) \gamma_5 u(p) = 0 \quad . \quad (28)$$

To summarize: The *ps* and *pv* matrix elements of an on-shell two-body operator, e.g. the T-matrix, can (in the positive energy sector) not be determined

uniquely by projection techniques. If the matrix elements are known *a priori*, as e.g. for the bare NN interaction V , of course no problems arise. The same holds when the Dirac sea is included in the formalism. The full information on the T-matrix is available and the Lorentz structure of the self-energy is then uniquely determined [9, 13, 14]. However, such an approach suffers from other problems (see next section). The ambiguity problem has e.g. been

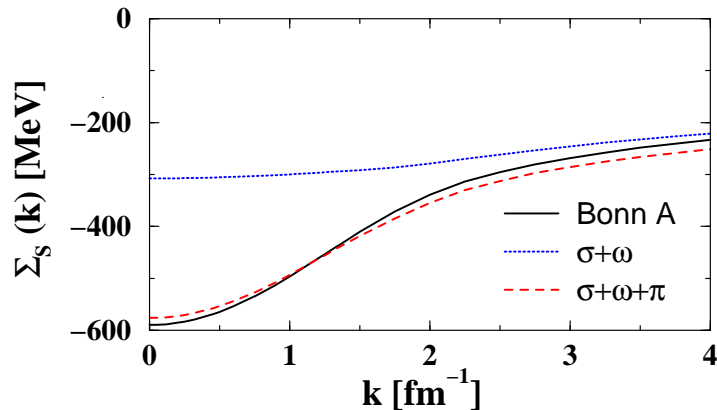


Fig. 3. Influence of the various meson exchange contributions on the nucleon self-energy (scalar part). The solid line corresponds to the full calculation (Bonn A), the dotted line to $\sigma\omega$ and the dashed line to $\sigma\omega\pi$ -exchange only. In all calculations the *pv* choice is used.

pointed out by Nuppenau et al. [15] and ter Haar and Malfliet [7] proposed a recipe to cure which was used by various groups: perform the projection, take the ps matrix element and replace it (due to physical reasons) by a pv one. This procedure was called the *pseudo-vector choice*. Later on, this procedure was critically examined by Fuchs et al. [11] and it was shown that it completely fails in controlling the leading order $1 - \pi$ -exchange contribution.

Fig. 3 shows the momentum dependence of the scalar self-energy component Σ_s at nuclear matter density $\rho = 0.166 \text{ fm}^{-3}$ obtained in the *pv* choice projection scheme, as it arises from the various meson exchange contributions of the Bonn A potential. Taking only σ and ω exchange into account the momentum dependence is flat inside the Fermi sea. Including the pion we are already very close to the full DBHF result. The strong momentum dependence of the present calculation originates to a large extent from pion-exchange.

It is a well known fact that a pseudo-scalar πNN coupling leads to extremely large pion contributions to the nuclear self-energy and contradicts soft pion theorems of ChPT [28]. Therefore in OBEPs always V_π with pseudo-

vector πNN coupling is used. It is, however, instructive to test the *pv choice* projection recipe for the case of the π -exchange [11]. This is done in Fig. 4 where the Hartree-Fock self-energy from the 1- π -exchange potential (OPEP) is shown. Exact results for a *ps* and *pv* πNN coupling can be compared to those obtained by projection techniques. It is seen that a *ps* description OPEP leads to extremely large self-energy components and a very strong momentum dependence. The *pv* coupling suppresses the V_π contribution by nearly two orders of magnitude and even on that scale the momentum dependence is much less pronounced. At the Hartree-Fock level the V_π self-energy can be computed directly or, alternatively, applying the same techniques as for the full T-matrix, i.e. going through the transformations from the $|LSJ\rangle$ basis to the helicity basis and finally via projection to the basis of covariant amplitudes. Doing so, it turns out that the *pv choice* projection fails to describe a *pv* pion exchange. Thus it is clear that the strong momentum dependence seen in the full self-energy (Fig. 3) is to large part due to spurious contributions from pseudo-scalar π -exchange. How these contributions can be eliminated has been discussed in [11] and [12] and is explained in more detail below.

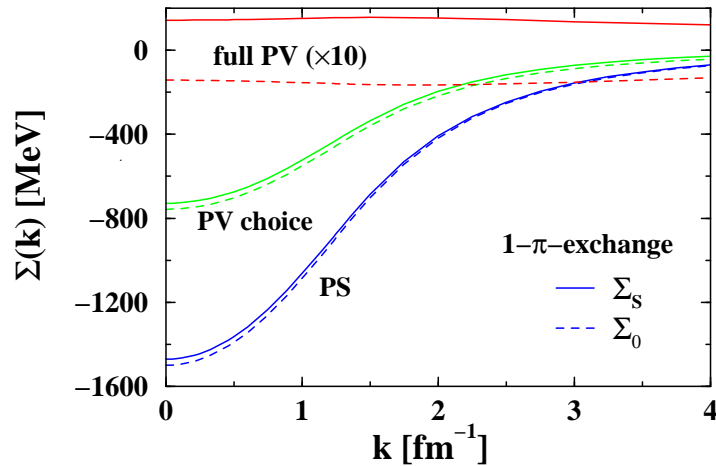


Fig. 4. Hartree-Fock self-energy originating from OPEP. results for V_π with *ps* and *pv* coupling are compared to results obtained within the *pv choice*. Solid lines represent the scalar, dashed lines the vector self-energy.

3.1 Covariant Representation of the T-Matrix

To use the trace formulas, Eqs. (8-10), one has to represent the T-matrix covariantly. A set of five linearly independent covariants is sufficient because

on-shell only five helicity matrix elements appear as solution of the Thompson equation. A linearly independent although not unique set of five covariants is given by the Dirac covariants

$$S = 1 \otimes 1, V = \gamma^\mu \otimes \gamma_\mu, T = \sigma^{\mu\nu} \otimes \sigma_{\mu\nu}, A = \gamma_5 \gamma^\mu \otimes \gamma_5 \gamma_\mu, P = \gamma_5 \otimes \gamma_5. \quad (29)$$

Using this special set, dubbed as *ps* representation in the following, the on-shell T-matrix for definite isospin I can be represented covariantly as [18]

$$T^I(|\mathbf{p}|, \theta, x) = F_S^I(|\mathbf{p}|, \theta, x)S + F_V^I(|\mathbf{p}|, \theta, x)V + F_T^I(|\mathbf{p}|, \theta, x)T \\ + F_A^I(|\mathbf{p}|, \theta, x)A + F_P^I(|\mathbf{p}|, \theta, x)P \quad . \quad (30)$$

Here \mathbf{p} and θ denote the relative three-momentum and the scattering angle between the scattered nucleons in the c.m. frame, respectively. The *direct* (Hartree) amplitudes are given by $\theta = 0$ and the *exchange* amplitudes (Fock) by $\theta = \pi$. The five covariant amplitudes F_i^I can be obtained by matrix inversion of eq. (30) from the five helicity amplitudes T^I . The nucleon self-energy in isospin saturated nuclear matter has then the form [10]

$$\Sigma_{\alpha\beta}(k, k_F) = \int \frac{d^3\mathbf{q}}{(2\pi)^3} \frac{\theta(k_F - |\mathbf{q}|)}{\tilde{E}^*(\mathbf{q})} [\tilde{m}_F^* 1_{\alpha\beta} F_S + \tilde{q}_{\alpha\beta}^* F_V] \quad , \quad (31)$$

where the isospin averaged amplitudes are defined as

$$F_i(|\mathbf{p}|, 0, x) := \frac{1}{2} [F_i^{I=0}(|\mathbf{p}|, 0, x) + 3F_i^{I=1}(|\mathbf{p}|, 0, x)] \quad . \quad (32)$$

Eq. (31) shows that the self-energy can be expressed solely in terms of direct scalar and vector amplitudes $F_{S,V}$, if these are derived from already anti-symmetrized helicity amplitudes (25) which obey the selection rule (24). Corresponding covariant exchange amplitudes $F_i^I(|\mathbf{p}|, \pi, x)$ are obtained from the exchange helicity amplitudes inverting a similar matrix for the exchange invariants $\tilde{S}, \tilde{V}, \tilde{T}, \tilde{A}, \tilde{P}$. The latter are related to the original invariants (29) through a Fierz transformation. The same Fierz transformation relates also direct and exchange amplitudes F_i . Thus the direct scalar and vector amplitudes $F_{S,V}$ in Eq. (31) contain already contributions from all other exchange amplitudes [27, 11].

Hence an explicit splitting of the already anti-symmetrized helicity amplitudes into direct and exchange parts $\frac{1}{2}(T^I(|\mathbf{p}|, 0, x) - T^I(|\mathbf{p}|, \pi, x))$ provides no additional information and is also not necessary. It becomes only relevant if one wants to replace the *ps* invariant by the *pv* invariant. However, now it becomes evident why the the above mentioned *pv choice* does not lead to the desired result: In this procedure the pseudo-scalar exchange amplitude $F_P^I(|\mathbf{p}|, \pi, x)$ is kept fixed and interpreted as a pseudo-vector one, replacing the corresponding invariant $\tilde{P} \mapsto \tilde{P}\tilde{V}$. Since the other amplitudes, due to Fierz, contain also *ps* contributions such an replacement is incomplete. As

can be seen from Fig. 4 the spurious ps contributions of the other amplitudes are still large.

To eliminate the such spurious pseudo-scalar contributions of the $1-\pi$ exchange completely one has to switch to another covariant representation of the T-matrix proposed by Tjon and Wallace [29] which we call *full pv* representation in the following

$$T^I(|\mathbf{p}|, \theta, x) = g_S^I(|\mathbf{p}|, \theta, x)S - g_{\tilde{S}}^I(|\mathbf{p}|, \theta, x)\tilde{S} + g_A^I(|\mathbf{p}|, \theta, x)(A - \tilde{A}) + g_{PV}^I(|\mathbf{p}|, \theta, x)PV - g_{\tilde{PV}}^I(|\mathbf{p}|, \theta, x)\tilde{PV} \quad . \quad (33)$$

The amplitudes $g^I(\theta)$ are explicitly given in [12]. In this scheme the pseudo-vector OPEP is exactly recovered. In Fig. 5 the corresponding self-energies

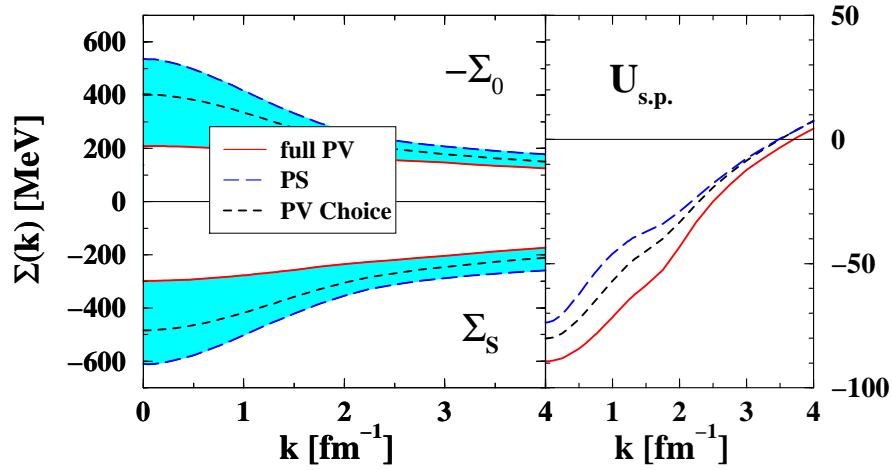


Fig. 5. Range of uncertainty spanned by the various decomposition schemes of the T-matrix for: self-energy components (left); single particle potential (right). The nuclear matter density is chosen as $\rho = 0.166 \text{ fm}^{-3}$ and the Bonn A potential is used.

obtained for the various decompositions are compared. Adopting the *full pv* representation, the space-like Σ_v contribution turns out to be much smaller than in the *ps* or the standard *pv choice*. Therefore we show the reduced self-energies $\tilde{\Sigma}_s$ and $\tilde{\Sigma}_o$ in which Σ_v is included for a better comparison. The pure *ps* and the *full pv* representation can be regarded as the limiting cases which give the range of uncertainty in the determination of the self-energy. The latter has the big advantage that this method ensures by construction a correct treatment of the *pv* OPEP at the Hartree-Fock level. Although the range of uncertainty is a few 100 MeV at the level of the self-energy

components, it drops out to most extent for *physical* observables which are based on complete matrix elements where vector and scalar parts contribute always with different sign. E.g., at the level of the single particle potential U the remaining uncertainty is only of about $10 \div 20$ MeV.

3.2 Covariant Representations of the Subtracted T-Matrix

The *full* pv representation successfully reproduces the HF nucleon self-energy for the pion exchange with pv coupling. However, as pointed out in [11], the *full* pv representation fails to reproduce the HF nucleon self-energy of other meson exchange potentials. Hence, it appears reasonable to treat the bare interaction V and the higher order ladder graphs of the T-matrix separately. Since the OBEPs are known analytically we can use a mixed representation of the form

$$V = V_{\pi,\eta}^{PV} + V_{\sigma,\omega,\rho,\delta}^P \quad . \quad (34)$$

Here the π - and η -amplitudes are treated by the decomposition (33) while for the $\sigma, \omega, \rho, \delta$ -amplitudes the ps representation (30) is applied. The higher order correlations of the T-matrix

$$T_{Sub} = T - V = i \int V Q G G T = \sum_{n=1}^{\infty} \int V (i Q G G V)^n \quad , \quad (35)$$

in the following called the subtracted T-matrix, can not be represented by such a mixed form since one can not disentangle the different meson contributions in the correlated ladder diagrams. The representation of the subtracted T-matrix remains therefore ambiguous. However, if the pion exchange contributes dominantly at the Hartree-Fock level a ps representation of the subtracted T-matrix should be more appropriate because of the higher order contributions of other meson exchanges. Thus the most favorable representation of the T-matrix is given by the ps representation

$$T^P = T_{Sub}^P + V_{\pi,\eta}^{PV} + V_{\sigma,\omega,\rho,\delta}^P \quad . \quad (36)$$

Here the ps representation for T_{Sub}^P is determined via the matrix elements

$$\langle \mathbf{p} \lambda'_1 \lambda'_2 | T_{Sub}^I(x) | \mathbf{q} \lambda_1 \lambda_2 \rangle := \langle \mathbf{p} \lambda'_1 \lambda'_2 | T^I(x) - V^I(x) | \mathbf{q} \lambda_1 \lambda_2 \rangle \quad , \quad (37)$$

with subsequently applying the projection scheme as in Eq. (30). An alternative representation of the T-matrix is given by a representation

$$T^{PV} = T_{Sub}^{PV} + V_{\pi,\eta}^{PV} + V_{\sigma,\omega,\rho,\delta}^P \quad , \quad (38)$$

where the subtracted T-matrix is represented by the *full* pv representation (33). This representation is similar to the *full* pv representation of the full T-matrix, however, with the advantage that now the pseudo-scalar contributions

in the bare nucleon-nucleon interaction, e.g. the $1-\omega$ exchange potential, are represented correctly.

In [12] the two representations (36) and (38) for the higher order ladder graphs were studied in detail. These two representations set the range of the remaining ambiguity concerning the representation of the T-matrix, i.e. after separating the leading order contributions. The outcome is the following:

- The dependence of the ladder kernel on the two different representation schemes is generally weak. This gives confidence that the ambiguities are to most extent removed as long as the leading Born term, in particular the pv OPEP, is treated correctly within the projection scheme.
- The momentum dependence of the self-energy is moderate and close to the *full* pv case shown in Fig. 5. This observation also justifies the *reference spectra approximation*.

Larger differences between the ps and pv representations of the ladder kernel occur only at high densities. Here the ps representation appears to be more appropriate. Therefore we consider this as the best solution of the problem. More details can be found in [12]. In this context it should be noted that in [30] the present subtraction scheme was extended to a special treatment of V_ρ where the tensor part leads also to a similar, but small on-shell ambiguity due to the Gordon identity.

4 Nuclear Matter

In this section I will discuss the role of correlations as well as implications of the various approximation schemes. Main emphasis will thereby be put on nuclear bulk properties, in particular on the nuclear equation-of-state (EOS), i.e. the binding energy per particle, and the nuclear saturation mechanism.

4.1 The Equation-of-State

In the relativistic Brueckner theory the energy per particle is defined as the kinetic plus half the potential energy

$$E/A = \frac{1}{\rho} \sum_{\mathbf{k}, \lambda} \langle \bar{u}_\lambda(\mathbf{k}) | \gamma \cdot \mathbf{k} + M + \frac{1}{2} \Sigma(k) | u_\lambda(\mathbf{k}) \rangle \frac{\tilde{m}^*(k)}{\tilde{E}^*(k)} - M \quad . \quad (39)$$

In Fig. 6 the EOSs, obtained in the various treatments, are compared. All calculations are based on the Bonn A interaction. First of all one sees that, except for a full ps treatment which is not correct for realistic potentials, the different calculations coincide at high densities. If one applies the *pv choice* the result is very close to that obtained by Brockmann and Machleidt (BM) [8]. This is somewhat surprising since there no projection scheme to the T-matrix has been applied but constant, i.e. momentum independent,

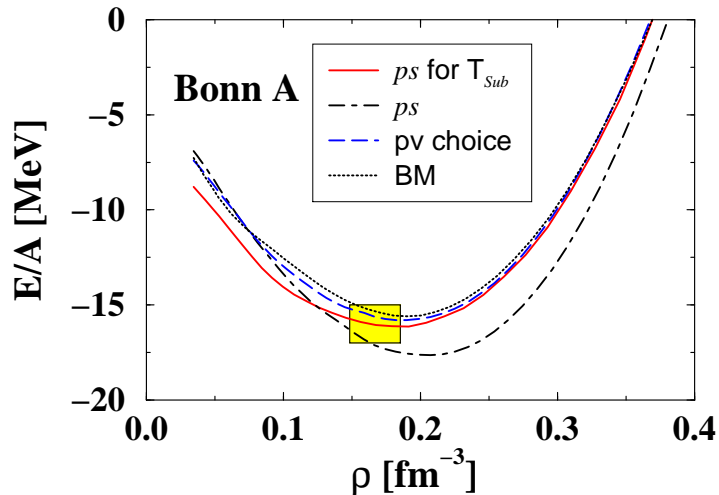


Fig. 6. Binding energy per particle as a function of nuclear matter density. As bare nucleon-nucleon interaction the Bonn A potential is used. For the T-matrix the subtraction scheme with the ps representation for the ladder kernel (solid) is compared to a ps representation of the full T-matrix (dash-dotted), to the pv choice and to the result of [8] (BM, dotted).

self-energy components have been determined by a fit to the single particle potential. As discussed in the previous sections the pv choice fails to reproduce the pv OPEP contribution to the self-energy. One can estimate this effect at the level of the binding energy by the comparison of the ps representation for the subtracted and the ps representation for the full T-matrix. In the latter case the nucleons are less bound at small densities. The situation changes, however, around saturation density. The full ps representation of the T-matrix contains maximal contributions from a pseudo-scalar πNN coupling which leads to saturation properties closer to non-relativistic Brueckner calculations (see below). A correct pseudo-vector representation of the pion, as used in the subtraction scheme, suppresses this effect. Thus at smaller densities one obtains a larger binding, while around saturation density the EOS is more repulsive.

In Fig. 7 we summarize the saturation points for iso-spin symmetric nuclear matter using different OBEPs as well as different approximation schemes. The saturation points for the two possible representations (36,38) for the subtracted T-matrix are very similar [12]. Therefore in the following I will consider the ps representation of the subtracted T-matrix as the optimal choice and compare this treatment with other works. With Bonn A one can reproduce the empirical saturation point of nuclear matter, shown as shaded region in the figure. The other Bonn potentials give less binding although

the saturation density is always close to the empirically known value. Compared to the calculations of Brockmann and Machleidt [8] our *Coester-line* is slightly shifted towards the empirical region which indicates that a refined treatment of the T-matrix leads to an enhancement of the binding energy connected with a reduced saturation density. In addition the result of ter Haar and Malfliet [7] based on the Groningen OBEP is shown. All results were obtained in the *no sea approximation*.

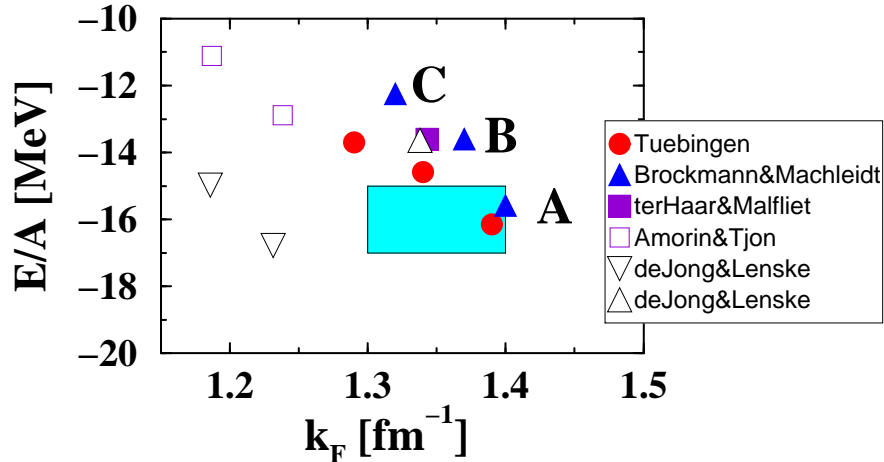


Fig. 7. Saturation points of nuclear matter, obtained with different OBEPs and within different approximation schemes. Full symbols correspond to standard relativistic Brueckner calculations, open symbols represent calculations which include Dirac sea contributions. The shaded area represents the empirical region of saturation.

A second group of points (open symbols in Fig. 7) includes explicitly negative energy states in the formalism. Here one has to keep in mind that standard OBEPs are derived within the *no sea approximation* and should therefore be used with caution in such calculations. The open triangle shows the result for Bonn C from [14] which is close to the corresponding Bonn C values of the standard treatment. Significant differences occur when OBEPs are used which were derived in full Dirac space. This is the case for the calculations of Amorin and Tjon [13] based on the Utrecht potential [31] and those of de Jong and Lenske [14] based on the Gross OBEP [32] (open triangles down). These results group at low densities which indicates strong additional repulsive components in the NN interaction resulting in a rather stiff EOS. As discussed in [14] the coupling to the Dirac-sea, in particular the coupling to nucleon-antinucleon pairs (*Z*-graphs) generates a strong dynamical repulsion. In contrast to standard OBEPs, where repulsive Dirac

sea contributions are effectively absorbed in a large ω coupling constant, OBEPs in full Dirac space generate such contributions dynamically. This is also reflected in a significantly reduced ω coupling constant. In nuclear matter the Dirac sea contributions experience a medium dependence, primarily through the reduction of the mass gap. Consequently, the Z -graph contributions are strongly enhanced at high densities which is the main source for the large repulsion observed in [13, 14]. Unfortunately, many-body calculations in full Dirac space show a strong sensitivity on off-shell effects, i.e. the corresponding form factors and to the three-dimensional reduction scheme of the BS-equation [14]. Here certainly more efforts would be needed to control the influence of the Dirac sea in the many-body dynamics with higher accuracy. It should be noticed that in non-relativistic treatments Dirac sea contributions can be accounted for on the level of three-body forces (see discussion below).

4.2 The Role of Correlations

In order to examine the role of correlations it is instructive to compare the full DBHF theory to the mean field picture. In relativistic mean field theory (MFT) [17, 33] saturation occurs generally through the interplay between the large attractive scalar field Σ_s , generated by the σ -meson, and the repulsive vector field Σ_o originating from the ω -meson. In MFT the vector field grows linear with density while the scalar field saturates at large densities which leads finally to saturation.

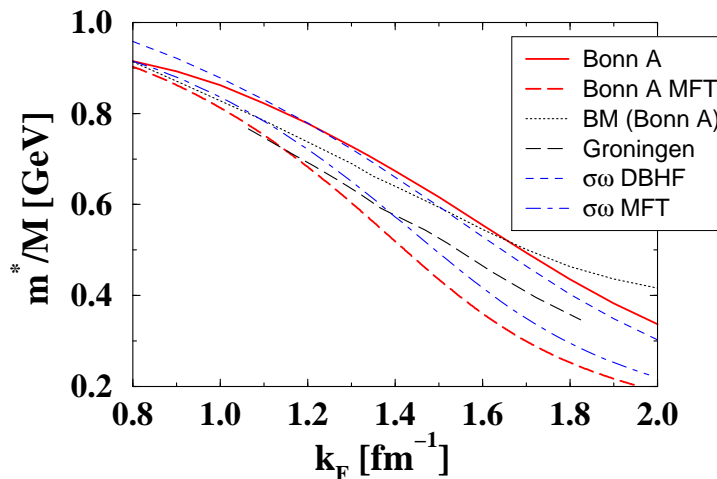


Fig. 8. The effective nucleon mass in the DBHF approach, using different NN interactions and approximation schemes, is compared to mean field calculations.

As an illustrative example Fig. 8 shows the density dependence of the effective nucleon mass \tilde{m}^* for various models: We compare the present DBHF result (Bonn A, ps for the subtracted T-matrix) to the mean field result for Bonn A. In the latter only σ and ω mesons contribute, exchange terms and contributions from other mesons vanish in iso-spin saturated nuclear matter [17, 33]. In addition DBHF results from other groups are shown, i.e. those of [8] (BM), a more recent calculation of the Groningen group [34], and the original calculation of Horowitz and Serot (HS) [18] using only σ and ω exchange. The corresponding MFT result is shown as well. In the latter two calculations the coupling constants of QHD-I [17], adjusted to nuclear matter instead to NN scattering, have been used. Remarkable is that all calculations, though partially based on quite different models, lead to the same qualitative behavior. This indicates that the decrease of \tilde{m}^* and its tendency to saturate at high densities is dictated by relativistic dynamics. The different DBHF calculations lie thereby within a band of about 100 MeV which is set by the usage of different OBEPs and different approximation schemes. The reason for this common behavior of \tilde{m}^* is easy to understand:

From eq. (31) it follows that the scalar self-energy (8) is determined by

$$\Sigma_s(\mathbf{k}, k_F) = \frac{4}{(2\pi)^3} \int d^3\mathbf{q} \frac{\tilde{m}_F^*}{\tilde{E}^*(\mathbf{q})} \theta(k_F - |\mathbf{q}|) F_S(\mathbf{k}, \mathbf{q}; k_F) . \quad (40)$$

In MFT the scalar amplitude F_S has to be replaced by the corresponding coupling constant of the scalar meson $(g_\sigma/m_\sigma)^2$. Eq. (40) represents then nothing else than the self-consistency equation for the effective mass

$$\Sigma_s(k_F) = -\frac{g_\sigma^2}{m_\sigma^2} \rho_S = -\frac{g_\sigma^2}{m_\sigma^2} \frac{4}{(2\pi)^3} \int d^3\mathbf{q} \frac{\tilde{m}_F^*}{\tilde{E}^*(\mathbf{q})} \quad (41)$$

which automatically leads to a saturating behavior for the attractive scalar field at large densities [17]. The momentum dependence of the T-matrix elements is generally moderate [30]. This explains also why DBHF results can well be approximated within density dependent mean field theory [20, 35] which means to replace F_S in (40) by an average value $\bar{F}_S(k_F)$. Also the variation of such average amplitudes with density is in general moderate, however, with a tendency to decrease with density. Hence, one leading effect for saturation which takes place on the scale of the large scalar and vector fields of a few hundred MeV is present in full DBHF theory as well as in MFT.

This does, however, not mean that the saturation mechanism is dominated by the mean field or Hartree contribution and exchange terms and higher correlations play only a minor role. The role of correlations can most easily be understood at the level of the two-nucleon wavefunction. As discussed e.g. in detail in [3, 30] and indicated in Fig. 2, correlations suppress the relative wavefunction at short distances. This reduces the short- and medium-range attraction of the σ -meson but even more effectively the short-range repulsion

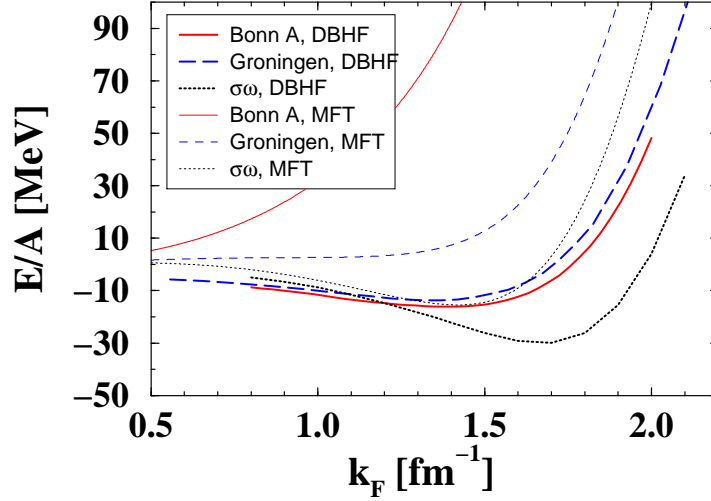


Fig. 9. The EOS obtained for various interactions in the DBHF approach is compared to mean field theory (MFT).

of the ω -meson. Correlation lead therefore, first of all, to a general reduction of the magnitude of the self-energies and, secondly, to a significant reduction of the repulsive components of the interaction. As can be seen from Fig. 9, at saturation density the scalar field is reduced by about 100 MeV compared to MFT and even more at higher densities. The same holds for the vector field. For realistic OBEPs the quenching of the repulsive ω exchange is essential for the saturation mechanism. In a pure mean field picture the system turns e.g. out to be unbound for Bonn A. When couplings are already adjusted to nuclear matter in MFT, as done in QHD-I where $g_\omega^2/4\pi = 10.84$ is about half of the Bonn A value $g_\omega^2/4\pi = 20$ while g_σ^2 is approximately the same, the higher order correlations lead to a significant softening of the EOS and shift the saturation point to higher densities [18]. This behavior is illustrated in Fig. 9 where DBHF results are compared to mean field calculations. The latter ones contain only contributions from σ and ω exchange, however, with the coupling strengths of the corresponding OBEPs Bonn A and Groningen. The calculations denoted by $\sigma\omega$ in Fig. 9 are in both cases based on $\sigma\omega$ exchange only, however, now with the corresponding couplings of QHD-I.

4.3 Role of the Pauli Operator

Another important in-medium effect is represented by the Pauli operator Q which projects the intermediate states in the BS-equation (2) onto unoccupied phase space areas. The influence of Pauli blocking on the dynamics is most clearly seen if one considers directly matrix elements or, respectively in-

medium cross sections [36, 37, 38, 39]. The differential on-shell cross section ($p = q$) is given by

$$d\sigma = \frac{(\tilde{m}^*)^4}{\tilde{s}^* 4\pi^2} |\hat{T}(q, q, \theta)|^2 d\Omega . \quad (42)$$

The squared matrix elements are obtained by the summation over 6 helicity helicity matrix elements (5 of them are independent) in the partial wave basis [23, 2, 39]. From (42) one sees first of all that, compared to free scattering in the medium appears a suppression factor $(\tilde{m}^*/M)^2$ which is solely due to kinematics. Furthermore, the Pauli operator modifies the optical theorem [38, 39] and damps in particular the imaginary part of the T-matrix which is directly proportional to Q (using R-matrix theory). For details see [39].

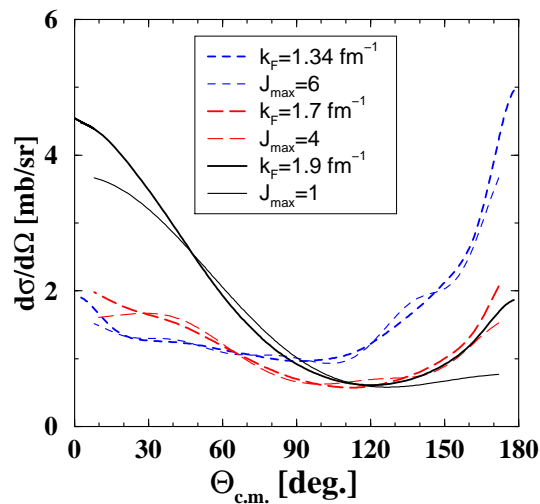


Fig. 10. Differential in-medium neutron-proton cross section for various densities at fixed laboratory energy of 250 MeV. The full results (thick lines) include partial waves up to $J = 12$ while the thin lines were obtained truncating higher partial waves.

Another important Pauli effect is the suppression of higher partial waves in the two-body correlations. This effect can be estimated from Fig. 10 where the medium dependence of the differential neutron-proton cross section (at $E_{\text{lab}} = 250$ MeV, using Bonn A) is displayed. The Fermi momenta correspond roughly to densities 1, 2, and 3 (in terms of $\rho_0 = 0.1625 \text{ fm}^{-3}$). The free np cross section is strongly forward-backward peaked. At moderate densities the presence of the medium tends to make the np differential cross section more isotropic. At backward angles the cross section are decreasing with density. At forward angles the behavior is more complicated: At moderate densities

the cross section is reduced but at high densities ($\rho = 2$ and $3\rho_0$) a strong enhancement of the forward scattering amplitude can be observed. Similar results have been obtained by Li and Machleidt [37]. At $3\rho_0$ the cross section turns out to be again highly anisotropic and to be dominated by a p -wave component. There occurs generally a suppression of higher partial waves with increasing density: At ρ_0 one needs partial waves up to at least $J \leq 6$ to approximate the full result ($J = 12$), at $2\rho_0$ the partial waves $J \leq 4$ are almost sufficient and at $3\rho_0$ the behavior is dominated by $s + p$ -waves.

It is quite natural that Pauli blocking is most efficient for the low momentum components of the interaction, generated mainly by iterated π -exchange, while high momentum components from iterated heavy meson exchange (σ, ω) are much less affected.

Another effect which is closely related to the Pauli operator is a possible onset of superfluidity at low densities. E.g. in the finite temperature approach of Alm et al. [38] a critical enhancement of the np cross section at low densities has been observed which was attributed to the onset of superfluidity. Crucial for such a superfluid state are contributions from hole-hole scattering in the Pauli operator ($Q = (1 - f - f)$) which are absent in the standard Brueckner approach ($Q = (1 - f)(1 - f)$). However, as discussed in [40] a signature of a bound pair state can appear at low densities even when hole-hole scattering is neglected in the Pauli operator. In [39] such an resonance like enhancement was seen in the amplitudes which correspond to the quantum numbers of the deuteron, i.e. the 3S_1 , 3D_1 and the 3S_1 - 3D_1 transition channels. Therefore the low density enhancement of the np cross section can be interpreted as a precursor of a superfluid state. The same effect has been discussed in [40].

5 Relativistic versus Non-Relativistic BHF

In contrast to relativistic DBHF calculations which came up in the late 80ies non-relativistic BHF theory has already almost half a century's history. The first numerical calculations for nuclear matter were carried out by Brueckner and Gammel in 1958 [4]. Despite strong efforts invested in the development of methods to solve the Bethe-Goldstone (BG) equation, the non-relativistic counterpart of the BS equation, it turned out that, although such calculations were able to describe the nuclear saturation mechanism qualitatively, they failed quantitatively. Systematic studies for a large variety of NN interactions showed that saturation points were always allocated on a so-called *Coester-line* in the $E/A - \rho$ plane which does not meet the empirical region of saturation. In particular modern OBEPs lead to strong over-binding and too large saturation densities where relativistic calculations do a much better job. Several reasons have been discussed in the literature in order to explain the success of the relativistic treatment. In the following I will recapitulate the main arguments for this difference.

5.1 Continuous Choice versus Gap Choice

Brueckner theory converges in terms of the hole-line expansion (for a recent review see [3]). In lowest order Brueckner theory (2 hole-lines) the effective 2-particle propagator in the BG-equation leads to a gap at the Fermi surface

$$iG_{12} = \frac{\bar{Q}}{\epsilon(\mathbf{q}) - E(\mathbf{k})} \quad (43)$$

with $\epsilon(\mathbf{q}) = U(k_F) + \frac{\mathbf{q}^2}{2m^*}$ the single particle energies below the Fermi momentum (starting energy) and $E(\mathbf{k}) = \frac{\mathbf{k}^2}{2M}$ the energy of the intermediate states above k_F . From (23) it is evident that the relativistic propagator does not contain such a gap. The continuous choice advocated by the Liege group [6] assumes the single particle potential to be valid also above k_F . This is in line with the relativistic propagator where fields are present below and above the Fermi momentum. Compared to the gap (or standard) choice the continuous choice shifts the Coester-line significantly towards the empirical region [41, 42]. It was further shown by the Catania group [43] that at the 3-hole-line level both choices lead to almost identical results. In the continuous choice already lowest order Brueckner theory (2-hole-lines) is very close to the result of the 3-hole-line expansion which suggests a faster convergence of the continuous choice.

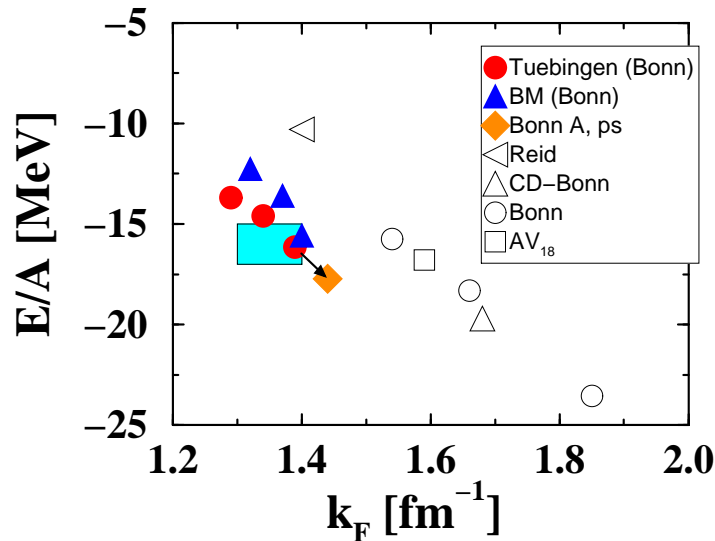


Fig. 11. Saturation points of relativistic (full symbols) versus non-relativistic (open symbols) BHF calculations (continuous choice).

5.2 Dirac Effects and Quenching of the Tensor Forces

The saturation mechanisms in relativistic and non-relativistic theories are quite different. In relativistic MFT the vector field grows linear with density while the scalar field saturates at large densities. In MFT this is the essential effect which leads to saturation. As discussed above, the density dependence of the scalar and vector DBHF self-energy is similar to MFT, however, exchange contributions and correlations lead a significant reduction of their absolute magnitude. A pure mean field picture works when σ and ω couplings are adjusted to nuclear matter, however, when fitted to free scattering data no saturation may occur at the mean field level, depending on the choice of the interaction. Exchange contributions and correlations are of crucial importance in order to obtain the saturation point at a scale which is set by the binding energy. A genuine feature of relativity, present in MFT as well as in DBHF, is the presence of large scalar and vector fields of a few hundred MeV size and a strongly decreasing effective nucleon mass with the tendency to saturate at high densities.

In the non-relativistic case the situation is quite different: The saturation mechanism takes place exclusively on the scale of the binding energy, i.e. a few ten MeV. It cannot be understood by the absence of a tensor force [44]. In particular the second order OPEP is large and attractive at high densities and its interplay with Pauli-blocking leads finally to saturation. Relativistically the interaction V receives a density dependence since matrix elements of V are built between in-medium spinors (16). As discussed in [45] the tensor interactions V_π , V_η and the Pauli part of V_ρ experience an additional reduction by the factor $(\tilde{m}^*/M)^2$. This reduction is at a first glance not completely obvious since it enters through the momentum dependence of second and higher order pseudo-vector OPE (and similar for η and ρ) where the range of the intermediate momentum \mathbf{k} is controlled by \tilde{m}^* . Consequently, the OPEP contribution to the binding energy is significantly reduced in the relativistic approach. Consistent with this observation is the present result (Figs. 6 and 11) obtained by a pure pseudo-scalar representation of the T-matrix within the projection scheme. As discussed above this leads to stronger weights of the self-energy contributions from pion exchange and in turn to stronger binding at higher density. It should, however, be kept in mind that in this calculation only the representation of the T-matrix is taken as ps , the V_π itself is still used with pv coupling.

In summary we have two genuine features of relativistic dynamics which are closely connected, act, however, at different scales: the saturation of the scalar attraction takes place on the scale of the large self-energy fields and the quenching of the tensor force at the scale of the binding energy. As argued in [45, 42] the latter effect is probably responsible for the improved Coester lines compared to BHF. In the language of effective field theory it may be tempting to relate this two scales with chiral fluctuations on top of large background fields originating from QCD condensates [46]. Remarkably, such

an approach can finally lead to very similar self-energies as the present DBHF calculations [46].

5.3 Resonance Degrees of Freedom and Three-Body Forces

Since the inclusion of explicit resonance degrees of freedom (DoFs) in the formalism is closely related to the occurrence of 3-body forces (3-BFs) I will discuss here both aspects in combination.

The most important resonance is of course the $\Delta(1232)$ isobar. At low and intermediate energies it provides large part of the intermediate range attraction and generates most of the inelasticity above the pion threshold. Intermediate Δ states appear in elastic NN scattering only in combination with at least two-isovector-meson exchange ($\pi\pi$, $\pi\rho$, ...) and give rise to a new class of box diagrams. As has been shown by the Bonn group [1] this class of diagrams can satisfactorily be absorbed into the effective σ -exchange. If the Δ is maintained as an explicit DoF in NN scattering, it provides additional attraction and the corresponding σ strength has to be readjusted. This leads e.g. in the work of the Groningen group to a reduction of $g_\sigma^2/4\pi = 7.4$ (w/o Δ) to $g_\sigma^2/4\pi = 6.4$ including Δ DoFs.

In many-body calculations explicit Δ DoFs give rise to additional saturation, shifting the saturation point away from the empirical region. This can be understood in the following way [47]: while the elementary σNN vertex is not modified in the medium, corresponding box diagrams with intermediate Δ and nucleon lines are affected. Dressing of the propagators and Pauli blocking of the nucleon state suppresses their contribution. Iterated to all orders, the maintenance of explicit Δ DoFs (instead of a stronger σ exchange) results therefore in less attraction. Quantitatively this effect has in detail been studied by ter Haar and Malfliet [7]. Fig. 12 shows the result of a more refined calculation from the Groningen group [48] which includes also the Δ self-energy. As one sees, the loss of binding energy is quite substantial. As pointed out in Refs. [3, 47] the inclusion of non-nucleonic degrees of freedom has to be performed with caution: Freezing out resonance DoFs generates automatically a class of three-body forces which contains nucleon-resonance excitations. 3-BFs with intermediate Δ excitations provide again a strong intermediate range attraction, $N^*(1440)$ excitations lead to small net repulsion [50]. Hence there exist strong cancellation effects between the repulsion due to box diagrams and contributions from 3-BFs. Such ring type diagrams of third and fourth order in the hole-line expansion have e.g. been conducted in [51]. A consistent treatment requires therefore to consider non-nucleonic DoFs and many-body forces on the same footing [47]. Many-body forces which are exclusively based on nucleon degrees of freedom can systematically be generated within chiral perturbation theory. Next to leading order all 3-BFs cancel [52] while non-vanishing contributions appear at NNLO [53].

Another class of 3-BFs which has extensively been studied within non-relativistic BHF involves virtual excitations of nucleon-antinucleon pairs.

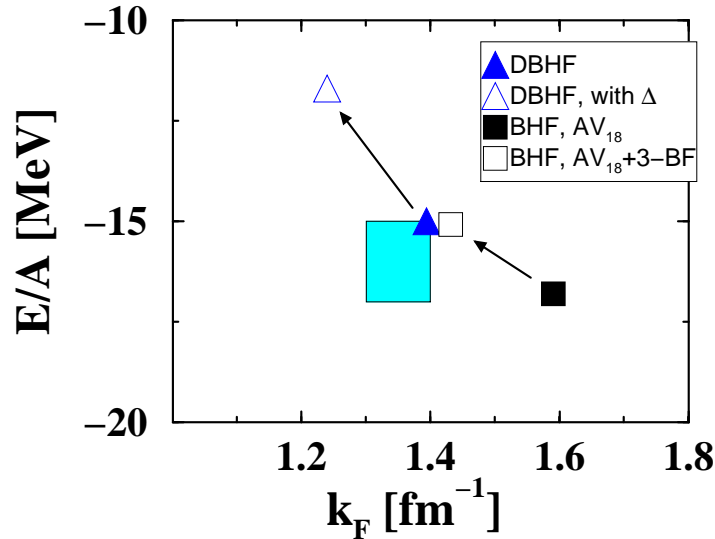


Fig. 12. Saturation points of DBHF calculations from the Groningen group without and including explicit Δ degrees of freedom [48], and of BHF calculations [49] based on the AV_{18} potential without and including 3-body forces.

Such Z-graphs are in net repulsive [50] and lead to a shift of the saturation point away from the non-relativistic Coester line towards its relativistic counterpart where the DBHF results are allocated. The calculation shown in Fig. 12 includes both, $\bar{N}N$ and as well as nucleon-resonance excitations [49].

It is often argued that in non-relativistic treatments 3-BFs play in some sense an equivalent role as the dressing of the two-body interaction by in-medium spinors in Dirac phenomenology. Both mechanisms lead indeed to an effective density dependent two-body interaction V which is, however, of different origin. In the medium 3-BFs can be considered as a renormalization of the meson vertices and propagators. Z-graphs are explicitly included when DBHF calculations are performed in full Dirac space, in the no sea approximation they are in some way effectively included through the usage of OBEPs with large ω couplings.

6 Summary

An overview on the present status of relativistic Brueckner calculations for the nuclear many-body problem was given. Using modern one-boson-exchange potentials such calculations provide a qualitatively satisfying - and parameter free - description of the nuclear saturation mechanism. Concerning the

extractions of the precise nuclear self-energy and its Lorentz structure there arise on-shell ambiguities due to lack of information on two-body matrix elements in full Dirac space when the approach is restricted to the positive energy sector (no sea approximation). A method to minimize the corresponding uncertainties was discussed.

Similar to relativistic mean field theory, Dirac phenomenology together with the structure of the NN interaction extracted from free scattering implies the existence of large scalar and vector fields. However, exchange contributions and higher order correlations reduce the magnitude of these fields compared to MFT and are essential for a quantitative saturation mechanism. When calculations are performed in full Dirac space part of the repulsion is generated from sea excitations which requires to renormalize the NN potentials. However, in the latter case the many-body dynamics can presently not be controlled with the same accuracy as in the standard approach based on the no sea approximation. In non-relativistic BHF nucleon-antinucleon excitations can be accounted on the level of three-body forces which leads to qualitatively similar results as in relativistic approach with solely two-body interactions. However, a consistent treatment of 3-BFs is a subtle problem which is closely connected to the introduction of non-nucleonic degrees of freedom, i.e. nuclear resonances. A future perspective would be the application of chiral NN potentials [54] where 3-BFs can consistently be by power counting. Another somewhat complementary challenge, relevant for the application to relativistic heavy ion reactions, is an extension to higher energies, using thereby high precision potentials above the pion threshold [55].

Acknowledgments

The author acknowledges valuable discussions with H. Lenske and W. Weise.

References

1. R. Machleidt, K. Holinde, Ch. Elster, Phys. Rep. **149**, 1 (1987)
2. R. Machleidt, Advances in Nuclear Physics **19**, 189, eds. J.W. Negele, E. Vogt (Plenum, N.Y., 1986).
3. H. Müther, A. Polls, Prog. Part. Nucl. Phys. **45**, 243 (2000)
4. K.A. Brueckner, J.L. Gammel, Phys. Rev. **107**, 1023 (1958)
5. F. Coester, S. Cohen, B.D. Day and C.M. Vincent, Phys. Rev. C **1**, 769 (1970)
6. J. P. Jeukenne, A. Lejeune, C. Mahaux, Phys. Rep. **25**, 83 (1976)
7. B. ter Haar and R. Malfliet, Phys. Rep. **149**, 207 (1987)
8. R. Brockmann, R. Machleidt, Phys. Rev. C **42**, 1965 (1990)
9. P. Poschenrieder, M.K. Weigel, Phys. Rev. C **38**, 471 (1988)
10. L. Sehn, C. Fuchs and A. Faessler, Phys. Rev. C **56**, 216 (1997)
11. C. Fuchs, T. Waindzoeh, A. Faessler and D.S. Kosov, Phys. Rev. C **58**, 2022 (1998)
12. T. Gross-Boelting, C. Fuchs, and A. Faessler, Nucl. Phys. A **648**, 105 (1999)
13. A. Amorin, J.A. Tjon, Phys. Rev. Lett. **68**, 772 (1992)
14. F. de Jong, H. Lenske, Phys. Rev. C **58**, 890 (1998)

15. C. Nuppenau, Y.J. Lee, A.D. MacKellar, Nucl. Phys. A **504**, 839 (1989)
16. H. Huber, F. Weber, and M.K. Weigel, Nucl. Phys. A **596**, 684 (1995)
17. B.D. Serot and J.D. Walecka, Advances in Nuclear Physics **16**, 1, eds. J.W. Negele, E. Vogt (Plenum, N.Y., 1986).
18. C.J. Horowitz and B.D. Serot, Nucl. Phys. A **464**, 613 (1987)
19. C.-H. Lee, T.S. Kuo, G.Q. Li, and G.E. Brown, Phys. Lett. B **412**, 235 (1997)
20. H. Lenske, C. Fuchs, Phys. Lett. B **345**, 355 (1995);
C. Fuchs, H. Lenske, H.H. Wolter, Phys. Rev. C **52**, 3043 (1995)
21. H. Shen, Y. Sugahara, and H. Toki, Phys. Rev. C **55**, 1211 (1997)
22. R.H. Thompson, Phys. Rev. D **1**, 110 (1970)
23. K. Erkelenz, Phys. Rep. C **13**, 191 (1974)
24. M. I. Haftel, F. Tabakin, Nucl. Phys. A **158**, 1 (1970)
25. M. Trefz, A. Faessler, W. H. Dickhoff, Nucl. Phys. A **443**, 499 (1985)
26. M. Rose, Elementary Theory of Angular Momentum (Wiley, N.Y., 1957).
27. J.A. Tjon and S.J. Wallace, Phys. Rev. C **32**, 1667 (1985)
28. S. Weinberg, Phys. Rev. Lett. **18**, 188 (1967); Phys. Rev. C **166**, 1568 (1966)
29. J.A. Tjon and S.J. Wallace, Phys. Rev. C **32**, 267 (1985)
30. E. Schiller, H. Mütter, Eur. Phys. J. A **11**, 15 (2001)
31. M.J. Zuilhof, J.A. Tjon, Phys. Rev. C **26**, 1277 (1982)
32. F. Gross, J.W. van Orden, K. Holinde, Phys. Rev. C **45**, 2094 (1992)
33. P. Ring, Prog. Part. Nucl. Phys. **73**, 193 (1996)
34. H.F. Boersma, R. Malfliet, Phys. Rev. C **49**, 233 (1994)
35. H. Lenske, this proceedings.
36. B. ter Haar, R. Malfliet, Phys. Rev. C **36**, 1611 (1987)
37. G.Q. Li and R. Machleidt, Phys. Rev. C **48**, 1702 (1993); *ibid* C **49**, 566 (1994).
38. T. Alm, G. Röpke, and M. Schmidt, Phys. Rev. C **50**, 31 (1994)
39. C. Fuchs, A. Faessler, M. El-Shabshiri, Phys. Rev. C **64**, 024003 (2001)
40. B.E. Vonderfecht, C.C. Gearhart, and W.H. Dickhoff, A. Polls, and A. Ramos, Phys. Lett. B **253**, 1 (1991).
41. H.J. Schulze, J. Cugnon, A. Lejeune, M. Baldo, U. Lombardo, Phys. Rev. C **52**, 2785 (1995)
42. M.K. Banerjee, J.A. Tjon, Nucl. Phys. A **708**, 303 (2002)
43. H.Q. Song, M. Baldo, G. Giansiracusa, U. Lombardo, Phys. Rev. Lett. **81**, 1584 (1998)
44. H.A. Bethe, Ann. Rev. Nucl. Sci. **21**, 93 (1971)
45. M.K. Banerjee, J.A. Tjon, Phys. Rev. C **58**, 2120 (1998)
46. P. Finelli, N. Kaiser, D. Vretenar, W. Weise, [arXiv:nucl-th/0205016]; *ibid.* [arXiv:nucl-th/0307069]
47. R. Machleidt, Int. J. Mod. Phys. B **15**, 1535 (2001) [arXiv:nucl-th/9911059]
48. F. de Jong, thesis, Groningen, 1992
49. W. Zuo, A. Lejeune, U. Lombardo, J.F. Mathiot, Nucl. Phys. A **706**, 418 (2002)
50. S.A. Coon, M.T. Pena, D.O. Riska, Phys. Rev. C **52**, 2925 (1995)
51. W.H. Dickhoff, A. Faessler, H. Mütter, Nucl. Phys. A **389**, 492 (1982)
52. S. Weinberg, Nucl. Phys. B **363**, 3 (1991)
53. U. van Klock, Phys. Rev. C **49**, 2932 (1994)
54. D.R. Entem, R. Machleidt, [arXiv:nucl-th/0304018]
55. H.V. von Geramb, A. Funk, H.F. Arellano, [arXiv:nucl-th/0105075]